

# Efficient Activation Quantization via Adaptive Rounding Border for Post-Training Quantization

**Zhengyi Li,<sup>1,2</sup> Cong Guo,<sup>1,2</sup> Zhanda Zhu,<sup>1</sup> Yangjie Zhou,<sup>1</sup> Yuxian Qiu,<sup>1,2</sup> Xiaotian Gao,<sup>3</sup> Jingwen Leng,<sup>1,2</sup> Minyi Guo<sup>1,2</sup>**

<sup>1</sup> Shanghai Jiao Tong University

<sup>2</sup> Shanghai Qi Zhi Institute

<sup>3</sup> Microsoft Research

{hobbit, guocong}@sjtu.edu.cn, zhanda.zhu@gmail.com, {yj.zhou, quiyuxian}@sjtu.edu.cn, xiaotian.gao@microsoft.com, leng-jw@sjtu.edu.cn, guo-my@cs.sjtu.edu.cn

## Abstract

Post-training quantization (PTQ) attracts increasing attention due to its convenience in deploying quantized neural networks. Rounding, the primary source of quantization error, is optimized only for model weights, while activations still use the rounding-to-nearest operation. In this work, for the first time, we demonstrate that well-chosen rounding schemes for activations can improve the final accuracy. To deal with the challenge of the dynamicity of the activation rounding scheme, we adaptively adjust the rounding border through a simple function to generate rounding schemes at the inference stage. The border function covers the impact of weight errors, activation errors, and propagated errors to eliminate the bias of the element-wise error, which further benefits model accuracy. We also make the border aware of global errors to better fit different arriving activations. Finally, we propose the AQuant framework to learn the border function. Extensive experiments show that AQuant achieves noticeable improvements with negligible overhead compared with state-of-the-art works and pushes the accuracy of ResNet-18 up to 60.31% under the 2-bit weight and activation post-training quantization.

## 1 Introduction

Despite the excellent accuracy performance of deep neural networks (DNNs), they have significant memory usage and computing costs. DNN quantization can reduce both computational and storage overhead by converting floating-point numbers into low-bit representations. It has become an effective technique for deploying DNNs on resource-limited devices. The quantization of DNNs can be further classified into two categories. Quantization-aware training (QAT) (Esser et al. 2019; Zhuang et al. 2021; Wang et al. 2019; Gong et al. 2019; Shen et al. 2021) trains quantized models from scratch on the full training dataset. Therefore, QAT is costly and time-consuming. Post-training quantization (Wang et al. 2020; Hubara et al. 2021; Banner, Nahshan, and Soudry 2019; Guo et al. 2021; Choi et al. 2021; Liu et al. 2021; Shomron et al. 2021; Nagel et al. 2020; Li et al. 2020) (PTQ) has recently attracted increasing interest due to its convenience and ease of deployment. It only requires a limited dataset (usually 1k images) to finetune a pre-trained model (Nagel et al. 2020; Li et al. 2020; Hubara et al. 2021).

Rounding is the most important source of error in quantization. Traditional quantization methods take the nearest rounding of each weight element, minimizing the mean squared error (MSE) between the quantized weight and the full-precision weight. AdaRound (Nagel et al. 2020) shows that a better solution is to learn the rounding scheme using the MSE of each layer’s output activation as the optimization objective. The subsequent BRECQ (Li et al. 2020) further expands the optimization granularity to the model block. So far, existing works have only considered rounding schemes of weights. The activation quantization still adopts the traditional rounding-to-nearest quantization. Adjusting activation rounding arises the challenge of runtime overhead. Existing works optimizing activation quantization sidestep this overhead by absorbing the effects of activation quantization into model weights (Nagel et al. 2019; Stock et al. 2020; Wei et al. 2022). But they regard activation errors as static perturbation and are hard to fit for different activations, leading to sub-optimal solutions. One fundamental sentiment of DNN quantization is that scalar multiplication errors (denoted as **element-wise error**) of the dot production cancel out each other so that the output error is trivial. However, nearest rounding of activations minimizes MSE of themselves, which is not equivalent to the output error. For varying activations, the element-wise error cannot always cancel out properly and lead to large output error.

To the best of our knowledge, this is the first work that studies the rounding scheme for the activation quantization. We first use a simple experiment to demonstrate that well-chosen rounding schemes for activations are beneficial to the final accuracy. Motivated by this, we theoretically derive that the optimization objective of activation rounding, which indicates it should consider the impact of weight quantization and the propagated error of previous layers. To minimize this objective, we make the element-wise errors unbiased by adaptive rounding border with negligible overhead. We further let the adjustment of border be aware of errors of other elements to better fit arriving activation vectors. Finally, equipped with the border function, we establish a PTQ framework AQuant that optimizes the border function to dynamically generate rounding schemes for activations at the inference stage. Extensive experiments on popular CNN models show that our method significantly outperforms the

recent state-of-the-art PTQ baselines with negligible extra parameters and computation overhead.

The contributions of this work are as follows:

1. We show the benefits of adjusting rounding schemes of activations both experimentally and theoretically, providing a new perspective for the post-training quantization.
2. To optimize the activation rounding, we design an efficient border function that produces unbiased element-wise errors, and make it can adjust to specific activations to generate adaptive rounding schemes. Based on this, we propose AQuant, a PTQ framework to optimize the border function.
3. We conduct comprehensive experiments on various CNN models using ImageNet. Under all the precision settings, our method greatly outperforms state-of-the-art PTQ methods, and the lower the number of bits, the more obvious the improvement. Specifically, the recovered accuracy of ResNet-18 on W2A2 (two-bit weight and activation) reaches 60.31%.

## 2 Preliminaries

**Notations.** The constant or scalar are denoted by italic letters, such as  $x_i$  and  $s$ . For layer  $\ell$ , we denote  $\mathbf{W}^{(\ell)}$  and  $\mathbf{w}^{(\ell)}$  as the weight tensor and its flattened version, respectively. Its input tensor is denoted by  $\mathbf{X}^{(\ell)}$ , and  $\mathbf{x}^{(\ell)}$  represents one column of it. We denote  $\mathbf{x}'^{(\ell)}$  as the noised version of  $\mathbf{x}^{(\ell)}$  caused by the quantization of previous layers.

For the convolutional layer, we denote the output channel, input channel, and the kernel size as  $o_c$ ,  $i_c$ , and  $k$ , respectively. The height and width of the input feature map are  $h_i$  and  $w_i$ , and  $h_o$  and  $w_o$  are the height and width of the output. In order to unify the feedforward of the convolution layer and the fully connected layer (FC) using matrix multiplication  $\mathbf{X}^{(\ell+1)} = \mathbf{W}^{(\ell)} \mathbf{X}^{(\ell)}$ , we explicitly convert the convolution filter from  $(o_c, i_c, k, k)$  to  $(o_c, i_c \times k \times k)$ . The input of convolutional layer is arranged from  $(i_c, h_i, w_i)$  to  $(i_c \times k \times k, h_o \times w_o)$  using `img2col` (Paszke et al. 2019). The  $h_o \times w_o$  is the number of sliding blocks, and each one have  $i_c \times k \times k$  elements in it. The activation function (ReLU) and the bias are omitted for simplicity. We denote  $\mathbb{E}[\cdot]$  as the expectation operator of  $\mathbf{x}$  on the dataset, and the network loss function is represented by  $\mathcal{L}(\cdot)$ .

**Quantization.** The uniform quantization and dequantization for the scalar  $x$  can be described as  $\hat{x} = s \cdot \text{clip}(\lceil x - B \rceil, \min, \max)$ , where  $s$  denotes the quantization scale step,  $\text{clip}(\cdot)$  is the clipping function.  $B$  is the rounding border, which we generalize its definition in this paper.

**Definition 2.1** (Rounding border). *Given the error function  $g(\Delta x)$ ,  $B$  is called as rounding border iff*

- the absolute error of rounding down equals to the one of rounding up, i.e.  $|g(-B)| = |g(1 - B)|$ .
- Any  $x$  with fractional part smaller than  $B$  should round down and vice versa.

Specially, traditional nearest rounding is when  $g(\cdot)$  is defined as self square error, and  $B$  is the constant 0.5.

Method	Bits	Res18	Res50	Reg600M
Baseline	W32A32	71.01	76.62	73.52
N-rounding	W32A2	40.22	21.13	6.10
A-rounding	W32A2	54.99	31.38	16.53

Table 1: Comparison of adjusted rounding (A-rounding) with nearest rounding (N-rounding).

## 3 Motivations

The basic operation of DNNs is vector dot production (**VDP**). Its output error is the accumulation of element-wise error of all additive components. A proper cancellation is important for a trivial output error. Previous works (Finkelstein, Almog, and Grobman 2019a; Nagel et al. 2020; Wei et al. 2022) apply nearest rounding to activations. Nearest rounding minimizes MSE of activations themselves, but is not aimed at the error cancellation. For varying activations, the element-wise error cannot always compensate as expected. In this work, we hypothesis adaptively adjusting the rounding schemes of activations can better cancel out the element-wise errors. To validate this, we conduct a simple experiment on three DNNs. The objective we adjust the activation rounding is to eliminate the mean shift of the vector after rounding. We optimize this because the mean error shift varies for different activation vectors and makes the output error biased (Finkelstein, Almog, and Grobman 2019a). The way we adjust the rounding is motivated by SQuant (Guo et al. 2021), a data-free PTQ method that makes the error sum of weights close to zero. We apply a similar idea to activations. More details are mentioned in the Appendix. We quantize activation to a low bitwidth to highlight the effectiveness and leave weights as full precision to exclude their impact. In Table 1, despite A-rounding does not consider the weight quantization or propagated errors, it still greatly outperforms the nearest rounding. A-rounding imposes heavy overhead at the inference stage and is impractical to use, but it motivates us to explore an effective and computationally efficient way to adjust activation rounding schemes.

## 4 Method

Motivated by the findings in Section 3, we first theoretically confirm that the rounding of activations should serve the output MSE of the following layer instead of themselves. Then the most challenging part of activation rounding is to dynamically adapt them at the inference stage. Learning static rounding schemes like those used in weights is difficult to handle dynamic activations, while complex rounding strategies are prevented by runtime overhead. To solve this dilemma, we first eliminate the bias of the element-wise error through an adaptive rounding border, so that their cancellation results in a smaller output error. Then we let the border adjust on the vector level to better fit in specific activations. With the designed border function, we establish a complete framework, AQuant, to optimize the border function and weight rounding schemes together.

## 4.1 Introducing Activation Quantization into the Optimization Objective

We now theoretically demonstrate that the rounding of activations should be dominated by the output MSE instead of themselves. We follow the assumption (a) of AdaRound (Nagel et al. 2020) that activations among different layers are much less relevant than activations within each layer to simplify the analysis. As such, we can analyze the perturbation of the activation in a layer-wise fashion. The effect of quantization error is formulated as

$$\begin{aligned} & \arg \min_{\Delta \mathbf{x}} \mathbb{E}[\mathcal{L}(\mathbf{x} + \Delta \mathbf{x}, \mathbf{y}, \mathbf{w}) - \mathcal{L}(\mathbf{x}, \mathbf{y}, \mathbf{w})] \\ & \stackrel{(a)}{\approx} \arg \min_{\Delta \mathbf{x}} \mathbb{E} \left[ \Delta \mathbf{x}^{(\ell)^T} \mathbf{g}^{(\mathbf{x}'^{(\ell)})} + \frac{1}{2} \Delta \mathbf{x}^{(\ell)^T} \mathbf{H}^{(\mathbf{x}'^{(\ell)})} \Delta \mathbf{x}^{(\ell)} \right] \\ & \approx \arg \min_{\Delta \mathbf{x}} \mathbb{E} \left[ \frac{1}{2} \Delta \mathbf{x}^{(\ell)^T} \mathbf{H}^{(\mathbf{x}'^{(\ell)})} \Delta \mathbf{x}^{(\ell)} \right], \end{aligned} \quad (1)$$

where  $\mathbf{g}^{(\mathbf{x}'^{(\ell)})}$  and  $\mathbf{H}^{(\mathbf{x}'^{(\ell)})}$  denote the first order derivative and Hessian matrix of the final loss  $\mathcal{L}$  w.r.t.  $\mathbf{x}'^{(\ell)}$ . The first term is ignored because the gradient term approaches 0 when the model gets converged (Nagel et al. 2020). Therefore, the second term defines the impact of the activation perturbation on the final loss  $\mathcal{L}(\mathbf{x}, \mathbf{y}, \mathbf{w})$ . Note that the inputs of layer  $\ell$  contain errors caused by the quantization of previous layers, so that we use noised  $\mathbf{x}'^{(\ell)} = \mathbf{x}^{(\ell)} + \mathbf{e}^{(\ell)}$  in Equation 5 instead of  $\mathbf{x}$ , and the  $\Delta \mathbf{x}^{(\ell)}$  is the difference between  $\hat{\mathbf{x}}'^{(\ell)}$  and  $\mathbf{x}^{(\ell)}$ . This **propagated error** is ignored by previous works (Nagel et al. 2020; Li et al. 2020; Wei et al. 2022), but it is important for adaptive activation rounding. Equation 1 cannot be directly optimized due to the computational complexity of the Hessian. We further expand the Hessian to find a way to approximate it. For two activations  $x_a^{(\ell)}$  and  $x_b^{(\ell)}$ , the corresponding element in Hessian is

$$H_{x_a^{(\ell)}, x_b^{(\ell)}}^{(\ell)} = \frac{\partial^2 \mathcal{L}}{\partial x_a^{(\ell)} \partial x_b^{(\ell)}} = \mathbf{W}_{:, b}^{(\ell)^T} \frac{\partial^2 \mathcal{L}}{\partial \mathbf{x}'^{(\ell+1)^2}} \mathbf{W}_{:, a}^{(\ell)}. \quad (2)$$

So that the Hessian matrix of activations  $\mathbf{x}'^{(\ell)}$  is

$$\mathbf{H}^{(\mathbf{x}'^{(\ell)})} = \mathbf{W}^{(\ell)^T} \frac{\partial^2 \mathcal{L}}{\partial \mathbf{x}'^{(\ell+1)^2}} \mathbf{W}^{(\ell)}. \quad (3)$$

The  $\frac{\partial^2 \mathcal{L}}{\partial \mathbf{x}'^{(\ell+1)^2}}$  requires backpropagation of second derivatives, which results in unbearable complexity. Nagel et al. (2020) shows that  $\frac{\partial^2 \mathcal{L}}{\partial \mathbf{x}'^{(\ell+1)^2}}$  is safe to be regarded as a diagonal constant matrix, denoted by  $\text{diag}(\nabla_{\mathbf{x}'^{(\ell+1)}}^2 \mathcal{L}_{i, i})$ . We have

$$\begin{aligned} & \arg \min_{\Delta \mathbf{x}} \mathbb{E} \left[ \Delta \mathbf{x}^{(\ell)^T} \mathbf{H}^{(\mathbf{x}'^{(\ell)})} \Delta \mathbf{x}^{(\ell)} \right] \\ & \stackrel{(b)}{=} \arg \min_{\Delta \mathbf{x}} \mathbb{E} \left[ \text{diag}(\nabla_{\mathbf{x}'^{(\ell+1)}} \mathcal{L}_{i, i}) \Delta \mathbf{x}^{(\ell)^T} \mathbf{W}_{i, :}^{(\ell)^T} \mathbf{W}_{i, :}^{(\ell)} \Delta \mathbf{x}^{(\ell)} \right] \\ & = \arg \min_{\Delta \mathbf{x}} \mathbb{E} \left[ \left( \mathbf{W}_{i, :}^{(\ell)} \Delta \mathbf{x}^{(\ell)} \right)^2 \right]. \end{aligned} \quad (4)$$

Here, (b) requires  $\Delta \mathbf{x}$  to be independently selected for different  $\mathbf{W}_{i, :}^{(\ell)}$ . The optimization of the final task loss decomposes into independent sub-problems in Equation 4. Each

sub-problem deals with the VDP of  $\mathbf{W}_{i, :}^{(\ell)}$  and  $\mathbf{x}'^{(\ell)}$ , resulting in a single expected value of the output tensor. This indicates that the quantization of activations is to minimize the output MSE of the next layer rather than the MSE themselves, which concludes our proof.

Nagel et al. (2020) has shown the quantization of weights should also minimize the output error. Then the optimization objective considering the quantization of both activations and weights is

$$\begin{aligned} & \arg \min_{\Delta \mathbf{x}', \Delta \mathbf{W}} \mathbb{E} \left[ \left( \left( \mathbf{W}_{i, :}^{(\ell)} + \Delta \mathbf{W}_{i, :}^{(\ell)} \right) \left( \mathbf{x}'^{(\ell)} + \Delta \mathbf{x}'^{(\ell)} \right) \right. \right. \\ & \quad \left. \left. - \mathbf{W}_{m, :}^{(\ell)} \mathbf{x}^{(\ell)} \right)^2 \right] \\ & = \arg \min_{\Delta \mathbf{x}', \Delta \mathbf{W}} \mathbb{E} \left[ \left( \left( \mathbf{W}_{i, :}^{(\ell)} + \Delta \mathbf{W}_{i, :}^{(\ell)} \right) \Delta \mathbf{x}'^{(\ell)} + \Delta \mathbf{W}_{m, :}^{(\ell)} \mathbf{x}'^{(\ell)} \right. \right. \\ & \quad \left. \left. + \mathbf{W}_{i, :}^{(\ell)} \mathbf{e} \right)^2 \right]. \end{aligned} \quad (5)$$

We eliminate full-precision  $\mathbf{x}^{(\ell)}$  since they are unknown at runtime. Equation 5 quantitatively shows that the rounding of activations should be aware of the impact of weight quantization and the propagated errors. We assume  $\Delta \mathbf{W}$  are given by the previous methods (Nagel et al. 2020; Li et al. 2020; Wei et al. 2022) since they are out of the scope of this work.

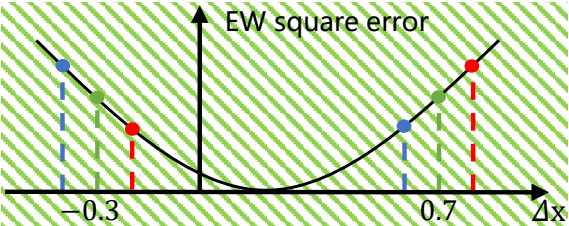
## 4.2 Adaptive Rounding Border

**Unbiased element-wise error.** Recall that in Section 3, eliminating the mean error shift of activations is beneficial. However, the output error in Equation 5 is the accumulation of element-wise errors of VDP. Besides activations, the element-wise errors are also effected by the weight quantization and propagated errors, so that merely eliminating mean error shift of activations is sub-optimal. A better way is to make the expected element-wise error unbiased. Then the element-wise error of different components are more evenly distributed on the two sides of zero, so that they can cancel out to a smaller and unbiased output error. Substituting the notation of Equation 5, the element-wise error of the VDP is

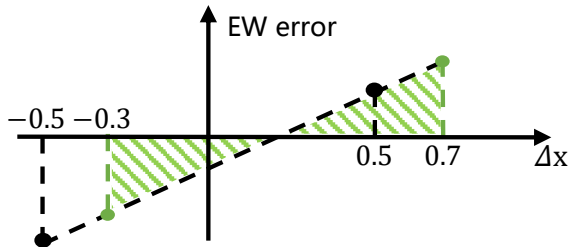
$$g(\Delta x') = (w + \Delta w) \Delta x' + \Delta w x' + w e, \quad (6)$$

where  $w$  and  $x'$  are one element of vector  $\mathbf{W}_{i, :}$  and its corresponding noised activation, and  $e$  is the propagated error. The weight is quantized offline and  $e$  is determined by previous layers. An important finding is that the Definition 2.1 holds for this error function. We give examples in Figure 1(a) to illustrate this. Suppose the  $w$ ,  $\Delta w$ ,  $e$  and  $x'$  together shape the square error of  $g(\Delta x')$ . Note that the curve actually moves for different fractional part of  $x'$ , but we assume it holds for easy illustration. In this case the rounding border is 0.3. The absolute element-wise error is the same for rounding pair  $\Delta x^- = -0.3$  and  $\Delta x^+ = 0.7$ . Any activations with fractional part smaller than 0.3 should round down (red pair) and vice versa (blue pair). Situations are the same for other combinations of  $w$ ,  $\Delta w$ ,  $e$  and  $x'$ .

With the modified border, one direct result is that we can obtain minimal element-wise error  $|g(\Delta x')|$ . Moreover, the modified border can make the expected element-wise error



(a) The element-wise square error function w.r.t.  $\Delta x$ . Dot lines with the same color represent one rounding pair with certain fractional part of  $x$ .



(b) The element-wise error function w.r.t.  $\Delta x$ . Without loss of generality, we assume the  $(w + \Delta w)$  is positive. The border  $B = 0.3$  results in unbiased element-wise error (green regions).

Figure 1: Illustration of the element-wise error.

unbiased. As illustrated in Figure 1(b), suppose the fractional part of  $x'$  uniformly distributes in the interval  $[0, 1]$ , the expected element-wise error is the integral of Equation 6. The expected value of nearest rounding is negative when taking integral from  $-0.5$  to  $0.5$ . On the contrary, the expected element-wise error is zero using the modified border (green region).

According to the central limit theorem, the optimization objective in Equation 5 benefits from the adaptive border from two aspects. The central limit theorem states the summation of independent random variables tends toward a normal distribution, despite their original distributions. The expected value and variance of the summation are the sum of the expected value and variance of these random variables, respectively. Previous studies have shown the values in DNNs can be approximated as independent (Kingma, Salimans, and Welling 2015). In this way, first, the expected value of the VDP error is also zero, so that it is not easy to accumulate or amplify (Finkelstein, Almog, and Grobman 2019a). Second, the square output error in Equation 5 is the variance of the VDP error when its expected value is zero. Since the adaptive border decreases the variance of each element-wise error, the square output error is also reduced.

The next problem is to efficiently obtain the rounding border at the inference stage. According to the definition of the rounding border, it satisfies  $|g(-B^E(x'))| = |g(1 - B^E(x'))|$ , which solves

$$B^E(x') = \frac{\Delta w}{(w + \Delta w)}x' + \frac{w}{(w + \Delta w)}e + \frac{1}{2}. \quad (7)$$

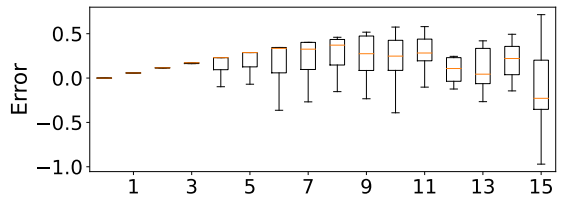


Figure 2: The propagated error w.r.t. the noised activation  $x'$ . For easy understanding, we group  $x'$  into 16 clusters according to their magnitude, as listed on the X-axis. Y-axis is the error between noised and full-precision activation.

We limit its range by  $\text{clip}(B^E(x'), 0, 1)$ . Compared to the constant border  $B = 0.5$  in nearest rounding,  $\frac{\Delta w x}{(w + \Delta w)}$  and  $\frac{w e}{(w + \Delta w)}$  quantitatively define the effects of weight quantization error and the propagation errors, respectively.

For the matrix multiplication of the convolutional layer, each  $x$  is corresponding to  $o_c$  sets of  $w$  and  $\Delta w$ , where  $o_c$  is the number of output channels. Although the optimal way is to assign a linear border function for each weight element, this introduces as many parameters as model weights, and is not acceptable in practice. We let the rounding scheme of  $x$  shared by the  $o_c$  weights. In this way, the first term of Equation 7 considers the effects of  $o_c$  weights. With this trade-off between extra parameter numbers and the performance, Aquant only imports  $O(\frac{1}{o_c})$  extra parameters compared with the model weights.

**Move to quadratic border function.** The quantization error of weights effect the rounding border linearly. The issue is that the contribution of the propagation error is unknown yet. Our profiling results on ResNet-18 under W2A4 quantization shows the propagated error is correlated to  $x'$ . For a pixel of the input of the second block, we summarize activation values and their errors on 1024 images, as shown in Figure 2. Consider the error in the sense of its mean value. As the magnitude of  $x'$  increases, the mean value first slowly deviates from zero, and then moves towards the opposite direction with faster rate. Similar trends are also observed on other pixels and other layers. To understand the reason of these two stages, consider the input vector that computes  $x'$ . The magnitude of  $x'$  is proportional to the magnitude of the input vector. In the first phase, as the magnitude of the input vector increases, for a given bitwidth, the input quantization error scales up, resulting in a large propagated error. In the second phase, clipping operation emerges more as the magnitude of input vector continues to increase. Clipping causes larger and always negative errors so that the mean value may change towards the opposite direction with a faster rate. We use a quadratic function w.r.t.  $x'$  to fit the propagated error, which does not introduce much computation or parameters. Absorbing the other two terms of Equation 7 into the quadratic function, the border function becomes

$$B^E(x) = b_2 \cdot x^2 + b_1 \cdot x + b_0, \quad (8)$$

where  $b_i$  are parameters learned through gradient descent on the calibration set.

---

Algorithm 1: Finetune pre-trained model block with rounding border function on one mini-batch

---

**Input:** Bit-width  $M$ , pre-trained model block composed by layer  $i$  to layer  $j$ , noised input  $\mathbf{X}'^{(i)}$  of layer  $i$  and FP output  $\mathbf{X}'^{(j+1)}$  of layer  $j$ ;  
**Output:** Border functions and weight schemes;  
1: **for**  $\ell = i$  to  $j$  **do**  
2:    $\hat{\mathbf{X}}'^{(\ell)} = s \cdot \text{clip}(\lceil \mathbf{X}'^{(\ell)} - B^{(\ell)}(\mathbf{X}'^{(\ell)}) \rceil, 0, 2^M - 1)$ ;  
3:    $\mathbf{X}'^{(l+1)} = (\mathbf{W}^{(\ell)} + \Delta \mathbf{W}^{(\ell)}) \hat{\mathbf{X}}'^{(\ell)}$ ;  
4: **end for**  
5: Compute MSE between  $\mathbf{X}'^{(j+1)}$  and  $\mathbf{X}'^{(j+1)}$  and do backward propagation;

---

**Border fusion.** Although the border achieves unbiased element-wise errors, they may still amplify for special combinations of activations. We hope the border to be aware of errors of other positions to better fit in specific cases. Since the border value is determined by the current activation, we simply take a weighted average for borders to integrate information. The activation vector is composed of  $i_c$  input channels, with each containing  $k^2$  elements. The intuitive way is to average the border on the whole vector. However, activations and weights from different input channels have varying scales. The gradient descent may only focus on input channels with large scales, which we find resulting in a bad local minimum. Therefore, we fuse the border separately for each input channel, which is

$$B^I(\mathbf{x}'_{ik^2:(i+1)k^2}) = \sum_{j=ik^2}^{(i+1)k^2-1} \frac{\alpha_j B_j^E(x'_j)}{k^2}, \quad (9)$$

where  $\mathbf{x}'_{ik^2:(i+1)k^2}$  is the  $i_{th}$  input channel of vector  $\mathbf{x}'$  and  $B_j^E$  is the border function of the pixel  $x_j$ .  $\alpha_j$  is also learned through gradient descent to adjust the importance of each element. In practice, the  $\alpha_j$  can be absorbed into  $B^E(\cdot)$ , but we write them explicitly to highlight their function. The border value is averaged and then shared within the input channel. This method may not be the optimal way to integrate global information, but it introduces no additional parameters and only adds one more average operation.

### 4.3 AQuant

Based on the effective and efficient border function in Equation 9, we finally propose AQuant. Substituting the  $\Delta \mathbf{W}$  by  $\lceil \mathbf{x}' - B(\mathbf{x}') \rceil - \mathbf{x}'$ , the optimization objective in Equation 5 becomes:

$$\min_{B(\cdot), \Delta \mathbf{W}} \mathbb{E} \left[ ((\mathbf{W} + \Delta \mathbf{W})(\lceil \mathbf{x}' - B(\mathbf{x}') \rceil) - \mathbf{W}\mathbf{x}' + \mathbf{W}\mathbf{e})^2 \right]. \quad (10)$$

The  $B(\mathbf{x}')$  here means to apply Equation 9 to each input channel of the sliding block. The optimization of weight rounding schemes follows previous methods (Wei et al. 2022) and we only denote as optimizing  $\Delta \mathbf{W}$  for simplicity. We use gradient descent to optimize the above formula for each model block, following Li et al. (2020); Wei et al.

(2022). Details of finetuning a block with adaptive border function are shown in Algorithm 1. For each block, it takes noisy inputs with all preceding layers quantized. Each layer in the block forwards with quantized activations and weights. Then we compute the MSE loss between quantized output and full-precision output, and update weight rounding schemes and border functions. We also design specific techniques to stable the optimization process of the border function, which we put in the appendix.

**Overhead Analysis.** We first analyze the extra parameter ratio of  $B(x)$  using the convolutional layer. For the reshaped convolutional filter with shape  $(o_c, i_c \times k^2)$ , since we let all output channels share the border function, we need  $i_c \times k^2$  sets of border functions. The quadratic function triples the number of extra parameter and results in  $3 \times i_c \times k^2$  parameters. Compared to the weight tensor that has  $o_c \times i_c \times k^2$  elements, the extra parameter ratio is  $3/o_c$ , which is very small due to the hundreds or thousands  $o_c$ .

Then we analyze the computing overhead. Taking the scalar multiplication as the basic operation, the complexity of the convolutional layer to compute an image is  $O(o_c \times i_c \times k^2 \times h_i \times w_i)$ . As for the border, for a total of  $i_c \times k^2 \times h_i \times w_i$  activations, the border function evaluates the quadratic function for each activation, requiring  $O(i_c \times k^2 \times h_i \times w_i)$  operations and is only  $O(1/o_c)$  compared to the innate computation of the layer. This ratio is also because the  $o_c$  weights share one border. Moreover,  $B(x)$  only includes element-wise computation and an average operation. Such a computation pattern is more efficient than the dominating operation of DNNs, matrix multiplication, in the sense of computing parallelism and memory access. The computation of border function can be easily fused with other kernels, such as `img2col` or the activation function ReLU. Even though we assign the border function a higher bitwidth than the backbone model, the overhead is still small enough to ignore, which we validate in Section 5.

## 5 Experiments

To verify the effectiveness of AQuant, we first compare AQuant with other SOTA PTQ approaches. Then we conduct ablation experiments and demonstrate the negligible overhead of AQuant.

**Experimental setup** Our algorithms are implemented using PyTorch (Paszke et al. 2019) and evaluated on Nvidia GPU V100. We optimize the border function using Adam optimizer (Kingma and Ba 2014) with learning rate 1e-3. For small models MobileNetV2 and MNasNet, we degrade the quadratic border to a linear border to reduce the extra parameter ratio. All the other settings and hyper-parameters are set the same as previous works (Nagel et al. 2020; Li et al. 2020; Wei et al. 2022) except the activation dropping, which disturbs the optimization of the rounding border. More detailed settings are described in the Appendix.

### 5.1 Comparison with SOTA Methods

To evaluate the effectiveness of AQuant, we conduct experiments on 6 CNN models using ImageNet (Deng et al. 2009)

Methods	Bits	Res18	Res50	MNV2
Baseline	FP	71.01	76.62	72.63
Rounding	W32A4	69.88	75.10	65.37
QDrop	W32A4	69.70	74.94	65.20
AQuant	W32A4	<b>70.12</b>	<b>75.69</b>	<b>68.78</b>
Rounding	W32A2	40.22	21.13	0.31
QDrop	W32A2	43.83	21.95	0.31
AQuant	W32A2	<b>62.09</b>	<b>61.59</b>	<b>2.20</b>
Methods	Bits	Reg600MF	Reg3.2GF	MNasx2
Baseline	FP	73.53	78.45	76.52
Rounding	W32A4	70.50	75.02	72.36
QDrop	W32A4	70.56	74.76	71.99
AQuant	W32A4	<b>72.06</b>	<b>77.44</b>	<b>74.19</b>
Rounding	W32A2	6.11	8.59	0.40
QDrop	W32A2	7.24	10.34	0.23
AQuant	W32A2	<b>44.27</b>	<b>55.95</b>	<b>13.24</b>

Table 2: Accuracy comparison on activation-only quantized models.

dataset, including ResNet-18 & 50 (He et al. 2016), MobileNetV2 (Sandler et al. 2018), MNasNet (Tan et al. 2019) and RegNet (Radosavovic et al. 2020). The models we use cover common designs of CNNs, including the residue connection, depthwise-separable convolution, and group convolution. To verify the effectiveness of AQuant on adjusting activation rounding, we only quantize the activations to exclude the impact of weights. As shown in Table 2, AQuant achieves significant improvements compared with nearest rounding and QDrop (Wei et al. 2022). QDrop optimizes the activation rounding error by considering it a static perturbation to weight. Therefore, their optimization is performed on weights and the performance is trivial when weights are full precision.

Then we present the results of fully-quantized models in Table 3. We compare AQuant with three strong baselines AdaRound (Nagel et al. 2020), BRECQ (Li et al. 2020), and QDrop (Wei et al. 2022). We report their results using the open-source codes. Our method outperforms previous PTQ methods in all cases. The benefits of AQuant become more prominent as the bitwidth decreases. For the challenging models like MobileNetV2 and MnasNet, we also achieve significant improvements compared with other methods. We find the ResNet-18 and ResNet-50 achieve more than 60% accuracy in the extremely low W2A2 quantization. It is worth noting that AQuant only has around 1% accuracy loss for 4-bit quantization on many models.

## 5.2 Ablation Study

**Border Function.** We verify the effectiveness of the quadratic border function in reducing the propagated error. We compare it with the linear border function. All settings except forms of border function are kept the same as in the previous section. As shown in Table 4, the quadratic border outperforms the linear border on both models and bitwidths.

Methods	Bits	Res18	Res50	MNV2
Baseline	FP	71.01	76.62	72.63
AdaRound	W4A4	69.49	74.82	67.53
BRECQ	W4A4	69.45	75.05	68.29
QDrop	W4A4	69.61	75.40	68.57
AQuant	W4A4	<b>70.03</b>	<b>75.58</b>	<b>69.15</b>
AdaRound	W2A4	63.64	66.61	44.90
BRECQ	W2A4	64.84	70.27	53.43
QDrop	W2A4	65.16	70.71	54.22
AQuant	W2A4	<b>66.63</b>	<b>71.11</b>	<b>56.74</b>
AdaRound	W3A3	66.00	69.72	48.92
BRECQ	W3A3	66.01	71.73	54.66
QDrop	W3A3	66.65	72.38	57.68
AQuant	W3A3	<b>67.97</b>	<b>73.20</b>	<b>58.56</b>
BRECQ	W2A2	51.12	51.36	7.44
QDrop	W2A2	54.19	57.38	11.45
AQuant	W2A2	<b>60.31</b>	<b>60.04</b>	<b>14.19</b>
Methods	Bits	Reg600MF	Reg3.2GF	MNasx2
Baseline	FP	73.53	78.45	76.52
AdaRound	W4A4	70.87	76.41	71.80
BRECQ	W4A4	70.96	76.64	73.24
QDrop	W4A4	71.19	76.76	73.54
AQuant	W4A4	<b>71.68</b>	<b>77.03</b>	<b>73.78</b>
AdaRound	W2A4	58.95	64.66	51.03
BRECQ	W2A4	62.41	71.21	62.11
QDrop	W2A4	63.59	71.34	63.78
AQuant	W2A4	<b>65.71</b>	<b>72.98</b>	<b>65.27</b>
AdaRound	W3A3	61.99	68.65	50.48
BRECQ	W3A3	63.79	71.75	64.16
QDrop	W3A3	65.37	72.69	66.43
AQuant	W3A3	<b>67.11</b>	<b>74.09</b>	<b>68.96</b>
BRECQ	W2A2	29.84	41.88	13.32
QDrop	W2A2	41.53	54.61	28.65
AQuant	W2A2	<b>46.61</b>	<b>57.48</b>	<b>30.31</b>

Table 3: Accuracy comparison on fully quantized models.

Methods	Strategy	Bits	Res18	Reg600M
Border function	Linear	W2A2	59.14	45.37
	Quadratic	W2A2	<b>60.31</b>	<b>46.61</b>
	Linear	W3A3	67.59	66.78
	Quadratic	W3A3	<b>67.97</b>	<b>67.11</b>
Border fusion	No fusion	W2A2	58.56	44.95
	Fusion	W2A2	<b>60.31</b>	<b>46.61</b>
	No fusion	W3A3	67.76	66.93
	Fusion	W3A3	<b>67.97</b>	<b>67.11</b>

Table 4: Impacts of border function and fusion.

**Border Fusion.** We then test the effectiveness of border fusion on error cancellation. ‘‘Fusion’’ is exact the AQuant mentioned in Section 4.3 and ‘‘No fusion’’ only uses the element-wise border function. According to Table 4, border fusion further improves the accuracy by error cancellation. On extreme low bitwidth, fusion produces more apparent improvements.

We find that the gap of both border function and border fusion shrink for 3-bit quantization because the effects of rounding errors get small. This also gives the freedom to use the linear border function or the element-wise function for high-bit quantization to save more overhead.

### 5.3 Overhead Analysis

**Ratio of AQuant parameters.** Existing works have shown 8-bit quantization can achieve almost lossless accuracy. In practice, the border function can be post quantized to 16 bits (Jacob et al. 2018). For ResNet-18 and ResNet-50, ratios of extra number of parameters are 0.81% and 0.64%, respectively. If weights utilize 4-bit quantization, AQuant only increases 3% of the model size. For RegNet-600MF and RegNet-3200MF, the ratios of the extra number of parameters are 2.82% and 2.14%, and the extra model size is around 10%. For small models MobileNetV2 and MNasNet, ratios of the extra number of parameters are 4.56% and 8.27%. The ratio of extra model size can be further reduced by training quantized border functions, such as 8-bit quantization.

**Runtime overhead.** As analyzed in the previous section, AQuant introduces only  $1/o_c$  extra computation complexity at the inference stage. Our profiling experiments show that the overhead is even more negligible due to the kernel fusion. We adopt element-wise border function  $B(x)$  since its improvement is enough in most cases. The convolution can be separated into two operators, `img2col` and `matmul`. We fuse the computation of  $B(x)$  with the `img2col` operator. Our implementation is based on the open-source code of Caffe (Jia et al. 2014) and is tested on Nvidia V100. Using batch size 32, we list the execution times of each layer of ResNet-18. As shown in Figure 3, executing times of fused convolution are close to the original times. On the whole model, the extra latency is 0.0028ms, which is only 5.11% of the original inference time.

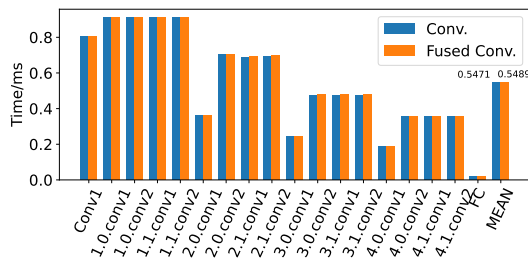


Figure 3: Latency breakdown on the ResNet-18. The experiment is executed 100 times and uses the average value.

## 6 Related Work

The quantization of deep neural networks can be classified into two categories. Quantization-aware Training (QAT) trains a quantized model on the full training dataset from scratch while Post-training quantization (PTQ) only requires a limited dataset (usually 1k images) to finetune a pre-trained model. Despite the promising accuracy reached by QAT (Esser et al. 2019; Wang et al. 2019; Gong et al. 2019; Shen et al. 2021), it suffers from the training costs and cumbersome hyper-parameter search. On the contrary, PTQ has been attracting a lot of interest due to its convenience. Studies include optimizing the clipping range of the weight (Choukroun et al. 2019; Banner, Nahshan, and Soudry 2019). Zhao et al. (2019) split channels to exclude outlier values, achieving lower bit quantization on the cost of extra computation. Other works include mix precision (Cai et al. 2020), synthetic data for PTQ (Zhang et al. 2021), and data-free quantization (Guo et al. 2021). AdaRound (Nagel et al. 2020) first theoretically proves that the nearest rounding, which minimizes the MSE of weight itself, is not optimal. Instead, they propose to learn the rounding scheme that minimizes the MSE of the layer output. BRECQ (Li et al. 2020) further proposes to reconstruct the weight blockwisely. However, these works and other works optimizing activation quantization (Esser et al. 2019; Nagel et al. 2019; Wei et al. 2022) apply the nearest rounding to activations, which we show is not optimal for the following inference. Larger errors may grow due to the dynamicity of activations.

Existing works tend to overlook the activation rounding due to the challenge to handle its dynamicity. They optimize the activation quantization from other aspects, such as learning the step size to minimize the MSE of activations themselves (Esser et al. 2019). Finkelstein, Almog, and Grobman (2019b); Nagel et al. (2019) compensate the mean activation shift by bias correction. But their optimization ignores the effects of model weights and is static. The most relevant work is QDrop (Wei et al. 2022). They highlight the importance of activation error and use weights to absorb it to import flatness, but at the cost of modeling activation errors statically. In this work, we adaptively adjust the rounding border according to varying activations at the inference stage.

## 7 Conclusion

This paper introduces AQuant, which makes up for the blank of activation rounding in PTQ algorithms. We theoretically show that the rounding of activations should serve the following computation. To efficiently round activations at runtime, we first demonstrate smaller output error can be achieved by using adaptive rounding border to generate unbiased element-wise error. On this basis, we further integrate global information for the border to better fit the arriving activations. The border function is incredibly lightweight and easy to compute at the inference stage. Extensive experiments on CNN models validate the efficiency of AQuant. It achieves higher accuracy on all kinds of bitwidths and significantly improves the low bitwidth, with negligible extra parameters and computation overhead.

## References

Banner, R.; Nahshan, Y.; and Soudry, D. 2019. Post training 4-bit quantization of convolutional networks for rapid-deployment. *Advances in Neural Information Processing Systems*, 32.

Cai, Y.; Yao, Z.; Dong, Z.; Gholami, A.; Mahoney, M. W.; and Keutzer, K. 2020. Zeroq: A novel zero shot quantization framework. In *Proceedings of the IEEE/CVF Conference on Computer Vision and Pattern Recognition*, 13169–13178.

Choi, K.; Hong, D.; Park, N.; Kim, Y.; and Lee, J. 2021. Qimera: Data-free Quantization with Synthetic Boundary Supporting Samples. In Ranzato, M.; Beygelzimer, A.; Dauphin, Y.; Liang, P.; and Vaughan, J. W., eds., *Advances in Neural Information Processing Systems*, volume 34, 14835–14847. Curran Associates, Inc.

Choukroun, Y.; Kravchik, E.; Yang, F.; and Kisilev, P. 2019. Low-bit quantization of neural networks for efficient inference. In *2019 IEEE/CVF International Conference on Computer Vision Workshop (ICCVW)*, 3009–3018. IEEE.

Deng, J.; Dong, W.; Socher, R.; Li, L.-J.; Li, K.; and Fei-Fei, L. 2009. ImageNet: A large-scale hierarchical image database. In *2009 IEEE Conference on Computer Vision and Pattern Recognition*, 248–255.

Esser, S. K.; McKinstry, J. L.; Bablani, D.; Appuswamy, R.; and Modha, D. S. 2019. LEARNED STEP SIZE QUANTIZATION. In *International Conference on Learning Representations*.

Finkelstein, A.; Almog, U.; and Grobman, M. 2019a. Fighting quantization bias with bias. *arXiv preprint arXiv:1906.03193*.

Finkelstein, A.; Almog, U.; and Grobman, M. 2019b. Fighting Quantization Bias With Bias. *CoRR*, abs/1906.03193.

Gong, R.; Liu, X.; Jiang, S.; Li, T.; Hu, P.; Lin, J.; Yu, F.; and Yan, J. 2019. Differentiable soft quantization: Bridging full-precision and low-bit neural networks. In *Proceedings of the IEEE/CVF International Conference on Computer Vision*, 4852–4861.

Guo, C.; Qiu, Y.; Leng, J.; Gao, X.; Zhang, C.; Liu, Y.; Yang, F.; Zhu, Y.; and Guo, M. 2021. SQuant: On-the-Fly Data-Free Quantization via Diagonal Hessian Approximation. In *International Conference on Learning Representations*.

He, K.; Zhang, X.; Ren, S.; and Sun, J. 2016. Deep residual learning for image recognition. In *Proceedings of the IEEE conference on computer vision and pattern recognition*, 770–778.

Hubara, I.; Nahshan, Y.; Hanani, Y.; Banner, R.; and Soudry, D. 2021. Accurate post training quantization with small calibration sets. In *International Conference on Machine Learning*, 4466–4475. PMLR.

Jacob, B.; Kligys, S.; Chen, B.; Zhu, M.; Tang, M.; Howard, A.; Adam, H.; and Kalenichenko, D. 2018. Quantization and training of neural networks for efficient integer-arithmetic-only inference. In *Proceedings of the IEEE conference on computer vision and pattern recognition*, 2704–2713.

Jia, Y.; Shelhamer, E.; Donahue, J.; Karayev, S.; Long, J.; Girshick, R.; Guadarrama, S.; and Darrell, T. 2014. Caffe: Convolutional architecture for fast feature embedding. In *Proceedings of the 22nd ACM international conference on Multimedia*, 675–678.

Kingma, D. P.; and Ba, J. 2014. Adam: A method for stochastic optimization. *arXiv preprint arXiv:1412.6980*.

Kingma, D. P.; Salimans, T.; and Welling, M. 2015. Variational dropout and the local reparameterization trick. *Advances in neural information processing systems*, 28.

Li, Y.; Gong, R.; Tan, X.; Yang, Y.; Hu, P.; Zhang, Q.; Yu, F.; Wang, W.; and Gu, S. 2020. BRECQ: Pushing the Limit of Post-Training Quantization by Block Reconstruction. In *International Conference on Learning Representations*.

Liu, Z.; Wang, Y.; Han, K.; Zhang, W.; Ma, S.; and Gao, W. 2021. Post-Training Quantization for Vision Transformer. In Ranzato, M.; Beygelzimer, A.; Dauphin, Y.; Liang, P.; and Vaughan, J. W., eds., *Advances in Neural Information Processing Systems*, volume 34, 28092–28103. Curran Associates, Inc.

Nagel, M.; Amjad, R. A.; Van Baalen, M.; Louizos, C.; and Blankevoort, T. 2020. Up or down? adaptive rounding for post-training quantization. In *International Conference on Machine Learning*, 7197–7206. PMLR.

Nagel, M.; Baalen, M. v.; Blankevoort, T.; and Welling, M. 2019. Data-free quantization through weight equalization and bias correction. In *Proceedings of the IEEE/CVF International Conference on Computer Vision*, 1325–1334.

Paszke, A.; Gross, S.; Massa, F.; Lerer, A.; Bradbury, J.; Chanan, G.; Killeen, T.; Lin, Z.; Gimelshein, N.; Antiga, L.; et al. 2019. Pytorch: An imperative style, high-performance deep learning library. *Advances in neural information processing systems*, 32.

Radosavovic, I.; Kosaraju, R. P.; Girshick, R.; He, K.; and Dollár, P. 2020. Designing network design spaces. In *Proceedings of the IEEE/CVF Conference on Computer Vision and Pattern Recognition*, 10428–10436.

Sandler, M.; Howard, A.; Zhu, M.; Zhmoginov, A.; and Chen, L.-C. 2018. Mobilenetv2: Inverted residuals and linear bottlenecks. In *Proceedings of the IEEE conference on computer vision and pattern recognition*, 4510–4520.

Shen, M.; Liang, F.; Gong, R.; Li, Y.; Li, C.; Lin, C.; Yu, F.; Yan, J.; and Ouyang, W. 2021. Once Quantization-Aware Training: High Performance Extremely Low-bit Architecture Search. In *Proceedings of the IEEE/CVF International Conference on Computer Vision*, 5340–5349.

Shomron, G.; Gabbay, F.; Kurzum, S.; and Weiser, U. 2021. Post-Training Sparsity-Aware Quantization. In Ranzato, M.; Beygelzimer, A.; Dauphin, Y.; Liang, P.; and Vaughan, J. W., eds., *Advances in Neural Information Processing Systems*, volume 34, 17737–17748. Curran Associates, Inc.

Stock, P.; Fan, A.; Graham, B.; Grave, E.; Gribonval, R.; Jegou, H.; and Joulin, A. 2020. Training with Quantization Noise for Extreme Model Compression. In *International Conference on Learning Representations*.

Tan, M.; Chen, B.; Pang, R.; Vasudevan, V.; Sandler, M.; Howard, A.; and Le, Q. V. 2019. Mnasnet: Platform-aware neural architecture search for mobile. In *Proceedings of*

*the IEEE/CVF Conference on Computer Vision and Pattern Recognition*, 2820–2828.

Wang, P.; Chen, Q.; He, X.; and Cheng, J. 2020. Towards accurate post-training network quantization via bit-split and stitching. In *International Conference on Machine Learning*, 9847–9856. PMLR.

Wang, Z.; Lu, J.; Tao, C.; Zhou, J.; and Tian, Q. 2019. Learning channel-wise interactions for binary convolutional neural networks. In *Proceedings of the IEEE/CVF Conference on Computer Vision and Pattern Recognition*, 568–577.

Wei, X.; Gong, R.; Li, Y.; Liu, X.; and Yu, F. 2022. QDrop: Randomly Dropping Quantization for Extremely Low-bit Post-Training Quantization. In *International Conference on Learning Representations*.

Zhang, X.; Qin, H.; Ding, Y.; Gong, R.; Yan, Q.; Tao, R.; Li, Y.; Yu, F.; and Liu, X. 2021. Diversifying sample generation for accurate data-free quantization. In *Proceedings of the IEEE/CVF Conference on Computer Vision and Pattern Recognition*, 15658–15667.

Zhao, R.; Hu, Y.; Dotzel, J.; De Sa, C.; and Zhang, Z. 2019. Improving neural network quantization without retraining using outlier channel splitting. In *International conference on machine learning*, 7543–7552. PMLR.

Zhuang, B.; Tan, M.; Liu, J.; Liu, L.; Reid, I.; and Shen, C. 2021. Effective training of convolutional neural networks with low-bitwidth weights and activations. *IEEE Transactions on Pattern Analysis and Machine Intelligence*.

# Efficient Activation Quantization via Adaptive Rounding Border for Post-Training Quantization

Anonymous submission

The following discussions are in the discrete space and we follow notations in the paper. Section A give details of the method used in the Motivation Section. Section B introduces designs of AQuant aiming at optimizing the border function. Section C mentions detailed setups of our experiments.

## A Experimental Setups of Section 3

Our method is motivated by SQuant (Guo et al. 2021). They minimize the constrained absolute sum of error of model weights. We apply similar ideas to activation vectors to eliminate their mean error shift. Consider a noised activation vector  $\mathbf{x}'$ , we reshape it as a matrix of shape  $(i_c, k^2)$  for easy illustration. The adjustment contains three steps. First, we apply nearest rounding to  $\mathbf{x}'$  and computes the rounding error  $\mathbf{r} = \hat{\mathbf{x}}' - \mathbf{x}'$ . Second, for  $i_{th}$  input channel  $\mathbf{x}'_{i,:}$ , the absolute value of error sum is  $s_i = |\sum_j r_{ij}|$ . Flipping one activation pluses one or minus one to the  $s_i$ . If the error sum is positive, we flip down either  $s_i$  or  $(s_i + 1)$  activations so that the  $s_i$  is smaller than 0.5. When adjusting the rounding schemes, we give priority to activations with fractional parts close to 0.5, since the element-wise impact of flipping them is the smallest. Third, we continue to consider the absolute value of the error sum of the whole  $\mathbf{x}'$ , which is  $p = |\sum_i s_i|$ . At this stage, all  $|s_i|$  are smaller than 0.5, and we only flip at most one activation of each input channel to maintain the constraint. Then each of  $p$  or  $p + 1$  input channels flips one activation to make the absolute value of the error sum of the whole vector smaller than 0.5.

## B Design of AQuant

**Refactor the Position of Activation Quantization Node.** The quantization pipeline of previous works (Nagel et al. 2020; Li et al. 2020; Wei et al. 2022) are shown in Figure 1(a). They apply rounding-to-nearest operation to activations as soon as they are generated, and then compute the mean square error (MSE) between  $\hat{\mathbf{x}}'^{(l+1)}$  and full-precision outputs  $\mathbf{x}'^{(l+1)}$ . However, according to the optimization objective of AQuant, the rounding of activations  $\mathbf{x}'^{(l)}$  should depend on the output MSE of the layer  $l$ . Therefore, we refactor the quantization pipeline to the one in Figure 1(b). The layer  $l$  accepts un-quantized activations as the input, and then AQuant adaptively quantizes activations at the begin-

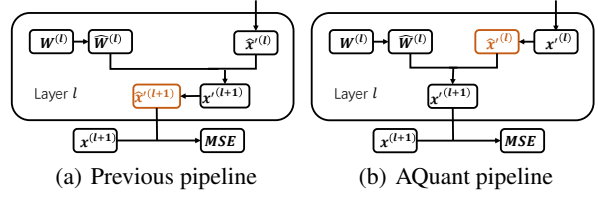


Figure 1: The position of activation quantization nodes of layer  $l$ . Positions of activation quantization are marked in a different color.

ning of layer  $l$ . After the forward, we compute MSE between un-quantized outputs and full-precision outputs.

One direct result of this refactor is that gradients of the activation quantization include the impact of weights, as shown in the following equation

$$\begin{aligned} \frac{\partial \text{MSE}}{\partial \mathbf{b}} &= \frac{\partial \text{MSE}}{\partial \mathbf{x}'^{(l+1)}} \frac{\partial \mathbf{x}'^{(l+1)}}{\partial \mathbf{b}} = \frac{\partial \text{MSE}}{\partial \mathbf{x}'^{(l+1)}} \frac{\partial \widehat{\mathbf{W}}^{(l)} \widehat{\mathbf{x}}'^{(l)}}{\partial \mathbf{b}} \\ &= \frac{\partial \text{MSE}}{\partial \mathbf{x}'^{(l+1)}} \widehat{\mathbf{W}}^{(l)} \frac{\partial \widehat{\mathbf{x}}'^{(l)}}{\partial \mathbf{b}} \end{aligned} \quad (1)$$

where  $\mathbf{b}$  are parameters related to the activation quantization, such as the border function  $B(\cdot)$  or the learned scale step (Esser et al. 2019). Note that we find that only the refactor can improve the accuracy without using AQuant through experiments. Our code is implemented based on the open source code of QDrop, which optimizes the scale step of activations. Such refactor improves the learned scale step by introducing the impact of weights. For example, using the open source codes of QDrop the accuracy is improved from 54.19 to 56.11 for ResNet-18 under W2A2 quantization.

**Bound the border range.** Since the border function may result in values beyond the interval  $[0, 1]$ , Section 4.2 writes that we clip them using  $\text{clip}(B^E(x'), 0, 1)$ . However, clipping is a non-differentiable operation. We use the sigmoid function instead to maintain the gradients. Without the constant term 0.5 in Equation 7, the impact of weight quantization and propagated errors should be bounded by the interval  $[-0.5, 0.5]$ , which is implemented using the sigmoid and a bias. Since this output is hard to approach -0.5 or 0.5 due to

the sigmoid, we scale the output value by a factor, which is 2.5 in our implementation. The sigmoid is also element-wise so that it can be fused with other operators with negligible overhead. In practice, the sigmoid can be substituted by any approximated function or by specific hardware.

**Rounding Schedule.** During the finetuning process, the changeable border causes the same activation leaps among rounding up and rounding down. The jumping rounding error makes the training process unstable. Therefore, we let the rounding error of activations be gradually introduced. Consider one noised activation  $x'$  and we let

$$\hat{x}' = \text{clip}(x' + \alpha(\lceil x' - B(x') \rceil - x'), \text{min}, \text{max}), \quad (2)$$

where  $\alpha$  controls the influence of rounding error. The  $\alpha$  equals 1 represents normal quantization while the  $\alpha$  equals 0 means no rounding error is introduced. AQuant sets  $\alpha$  as 0 for the first 20% finetuning iterations and then lets  $\alpha$  linearly approach 1 as the finetuning goes on.

## C More Experimental Setups

Besides the settings mentioned in Section 5, we keep most of the settings the same as other baselines (Nagel et al. 2020; Li et al. 2020; Wei et al. 2022). The first and the last layer are kept in 8-bit. The calibration set contains 1024 random images from ImageNet (Deng et al. 2009) and we finetune each block or layer for 20k iterations with batch size 32. To maintain the gradient of parameters of the border function, we substitute the rounding operation by straight-through estimator (STE) (Bengio, Léonard, and Courville 2013). Learning rate for the activation step size is 4e-5 and for the weight rounding is 3e-3. Other different settings are mentioned below.

**Convergence of the Weight Rounding Scheme.** Previous works use soft quantization variables  $h(\mathbf{V})$  to learn the rounding scheme of weights

$$\mathbf{W}' = s \cdot \text{clip} \left( \left\lfloor \frac{\mathbf{W}}{s} \right\rfloor + h(\mathbf{V}), \text{min}, \text{max} \right). \quad (3)$$

The function  $h(\cdot)$  is a rectified sigmoid proposed in Louizos, Welling, and Kingma (2017) and  $V$  is regularized by

$$f_{reg}(\mathbf{V}) = \lambda \left( \sum_{i,j} 1 - |2h(\mathbf{V}_{i,j}) - 1|^\beta \right), \quad (4)$$

where  $\lambda$  is the harmony coefficient balancing the regularization and the output mean square error (MSE). They anneal the parameter  $\beta$  to gradually learn the rounding scheme. A higher  $\beta$  allows  $h(\mathbf{V})$  to freely adapt to improve the output MSE. As the finetuning process goes on,  $\beta$  gradually decreases to encourage  $h(\mathbf{V})$  to converge to 0 or 1, which finally arrives at the binary solution. Specifically, the  $\beta$  begins at 20 and finally decreases to 2 and the  $\lambda$  is set as 0.01 in their works. Through experiments, we find importing AQuant slows down the convergence of  $h(\mathbf{V})$  due to the flipping of activation rounding. Since we keep the same number of finetuning iterations, for these layers, we let the  $\beta$  starts with 16 and set  $\lambda$  as 0.05 to enhance the regularization of weight rounding.

**The substitution of QDrop** Our implementation is based on the open source code of QDrop (Wei et al. 2022), another work optimizing the quantization error of activations. The main idea of QDrop is to find a flat minimum by randomly dropping the quantization of activations during finetuning. Dropping quantization means they substitute the noised activations with full-precision activations. QDrop finetunes the pre-trained model on the block level. Two types of dropping contribute to their improvements. The first is to drop the quantization of the block input and the second is to drop the quantization of intermediate activations within the block. In AQuant, only the dropping of block input is adopted. This is because dropping the quantization of intermediate activations changes the activation distribution and may mislead the optimization of the border function.

## References

Bengio, Y.; Léonard, N.; and Courville, A. 2013. Estimating or propagating gradients through stochastic neurons for conditional computation. *arXiv preprint arXiv:1308.3432*.

Deng, J.; Dong, W.; Socher, R.; Li, L.-J.; Li, K.; and Fei-Fei, L. 2009. ImageNet: A large-scale hierarchical image database. In *2009 IEEE Conference on Computer Vision and Pattern Recognition*, 248–255.

Esser, S. K.; McKinstry, J. L.; Bablani, D.; Appuswamy, R.; and Modha, D. S. 2019. LEARNED STEP SIZE QUANTIZATION. In *International Conference on Learning Representations*.

Guo, C.; Qiu, Y.; Leng, J.; Gao, X.; Zhang, C.; Liu, Y.; Yang, F.; Zhu, Y.; and Guo, M. 2021. SQuant: On-the-Fly Data-Free Quantization via Diagonal Hessian Approximation. In *International Conference on Learning Representations*.

Li, Y.; Gong, R.; Tan, X.; Yang, Y.; Hu, P.; Zhang, Q.; Yu, F.; Wang, W.; and Gu, S. 2020. BREQC: Pushing the Limit of Post-Training Quantization by Block Reconstruction. In *International Conference on Learning Representations*.

Louizos, C.; Welling, M.; and Kingma, D. P. 2017. Learning sparse neural networks through  $L_0$  regularization. *arXiv preprint arXiv:1712.01312*.

Nagel, M.; Amjad, R. A.; Van Baalen, M.; Louizos, C.; and Blankevoort, T. 2020. Up or down? adaptive rounding for post-training quantization. In *International Conference on Machine Learning*, 7197–7206. PMLR.

Wei, X.; Gong, R.; Li, Y.; Liu, X.; and Yu, F. 2022. QDrop: Randomly Dropping Quantization for Extremely Low-bit Post-Training Quantization. In *International Conference on Learning Representations*.